ornl

ORNL/TM-10698

OAK RIDGE
NATIONAL
LABORATORY

MARTIN MARIETTA

H_α Monitors for the Advanced Limiter Test-II (ALT-II) on TEXTOR

Taner Uckan

OAK RIDGE NATIONAL LABORATORY
CENTRAL RESEARCH LIBRARY
CIRCULATION SECTION
4500N ROOM 175
LIBRARY LOAN COPY
DO NOT TRANSFER TO ANOTHER PERSON
If you wish someone else to see this report, send in name with report and the library will arrange a loan.

OPERATED BY
MARTIN MARIETTA ENERGY SYSTEMS, INC.
FOR THE UNITED STATES
DEPARTMENT OF ENERGY

Printed in the United States of America. Available from
National Technical Information Service
U.S. Department of Commerce
5285 Port Royal Road, Springfield, Virginia 22161
NTIS price codes—Printed Copy: A03; Microfiche A01

This report was prepared as an account of work sponsored by an agency of the United States Government. Neither the United States Government nor any agency thereof, nor any of their employees, makes any warranty, express or implied, or assumes any legal liability or responsibility for the accuracy, completeness, or usefulness of any information, apparatus, product, or process disclosed, or represents that its use would not infringe privately owned rights. Reference herein to any specific commercial product, process, or service by trade name, trademark, manufacturer, or otherwise, does not necessarily constitute or imply its endorsement, recommendation, or favoring by the United States Government or any agency thereof. The views and opinions of authors expressed herein do not necessarily state or reflect those of the United States Government or any agency thereof.

ORNL/TM-10698
Dist. Category UC-421, 424, 426

Fusion Energy Division

H_α MONITORS FOR THE ADVANCED LIMITER TEST–II (ALT-II) ON TEXTOR

Taner Uckan

Date published: May 1988

Prepared by the
OAK RIDGE NATIONAL LABORATORY
Oak Ridge, Tennessee 37831
operated by
MARTIN MARIETTA ENERGY SYSTEMS, INC.
for the
U.S. DEPARTMENT OF ENERGY
under contract DE-AC05-84OR21400

MARTIN MARIETTA ENERGY SYSTEMS LIBRARIES
3 4456 0276315 0

CONTENTS

ACKNOWLEDGMENTS iv
ABSTRACT v
I. INTRODUCTION 1
II. ALT-II PUMP LIMITER SYSTEM 3
III. H_α MONITOR LAYOUT 3
IV. MODEL FOR ESTIMATING PARTICLE FLUX 7
V. MONITOR CALIBRATION 13
VI. MEASUREMENT PARAMETERS ON TEXTOR 15
A. ALT-II Performance Studies 16
B. Particle Balance Studies and Recycling 17
C. Global Particle Confinement Time 18
VII. MONITOR LOCATIONS ON TEXTOR 20
VIII. EXPERIMENTAL OBSERVATIONS AND RESULTS 20
IX. DISCUSSIONS 27
REFERENCES 28

ACKNOWLEDGMENTS

The author thanks the members of the ALT-II group from TEXTOR and the University of California at Los Angeles for their support and collaboration on this task, especially K. H. Dippel, K. H. Finken, D. M. Goebel, A. Pospieszczyk, U. Samm, and H. Soltwisch, who made available the plasma density data, and W. Kohlhaas, who provided help in the design and fabrication of the monitor viewing ports on the device. The continuous encouragement from and the valuable discussions with P. K. Mioduszewski and the help of G. R. Dyer on the monitor electronics are gratefully acknowledged.

ABSTRACT

The H_α monitor system installed on TEXTOR in conjunction with the Advanced Limiter Test–II (ALT-II) toroidal belt pump limiter is introduced. The monitors are used to study edge particle fluxes and recycling, correlations to confinement properties of core and edge plasma with ALT-II, and also high-power auxiliary heating (~5 MW) during long-pulse (~4-s) operation of TEXTOR. A model of the edge particle flux based on the H_α measurements is presented. The ALT-II experiments are to be carried out in various phases. Here we discuss the results obtained from the monitor system during the initial phase of operations following the installation of the ALT-II limiter, with ohmic heating only.

I. INTRODUCTION

In general, a pump limiter can control the plasma density only by removing a small percentage of the particles that would otherwise be recycled after hitting the wall of the vacuum chamber or the limiter. Already, for example, the Impurity Study Experiment (ISX) pump limiter[1] and the Advanced Limiter Test–I (ALT-I) modular pump limiter[2] on the TEXTOR tokamak have successfully demonstrated such density control. Recently the ALT-II toroidal belt pump limiter[3] was installed on TEXTOR.[4] To evaluate the performance of ALT-II on TEXTOR, the edge plasma fluxes and their recycling in time and space must be measured and monitored during the pump limiter experiments. A conventional diagnostic for studying the particle recycling is monitoring of the Balmer alpha (H_α) emission from the edge of the plasma. This radiation results from the collisional excitation of a neutral hydrogen (deuterium) atom from the device wall or limiter surfaces when it enters the plasma. These measurements are made with optical H_α diagnostics in various locations on TEXTOR. The tasks of fully implementing these diagnostics on the device and carrying out the measurements and data evaluations during the ALT-II experiments are the responsibility of the Plasma-Materials Interactions Group of Oak Ridge National Laboratory (ORNL) in collaboration with the University of California at Los Angeles and TEXTOR staff members. The ALT-II experiments will be carried out in several phases. Figure 1 contains the experimental program outline with respect to other belt limiter and modular pump limiter experiments in major tokamaks and the expected schedule.[5]

TEXTOR[4] is a medium-sized tokamak with a major radius $R_0 = 175$ cm, a minor radius $a = 40$–48 cm, a liner located at $a_w = 55$ cm, a toroidal field $B = 2$ T, and a typical plasma current $I_p = 350$ kA, corresponding to an edge safety factor $q(r = 46 \text{ cm}) = 3.5$. Most of the plasma runs are with prefill gas only. A typical discharge duration is ~3.5 s, with an electron density $n_e \sim 3 \times 10^{13}$ cm^{-3} and temperature $T_e \sim 800$ eV. Core and edge plasma parameters are summarized in Table 1. The device liner is kept at elevated temperature, about 300°C, but all viewing ports are water cooled and their temperature typically stays around 40°C. The TEXTOR limiter system consists of an ion cyclotron heating (ICH) antenna limiter at $r = 48.5$ cm and a main limiter with one segment about 60 cm wide on the inner wall at $r = 48$ cm; the other three limiters are 30 cm wide in the poloidal direction, about 10 cm in the toroidal direction, and movable from $r = 40$ to 48 cm.

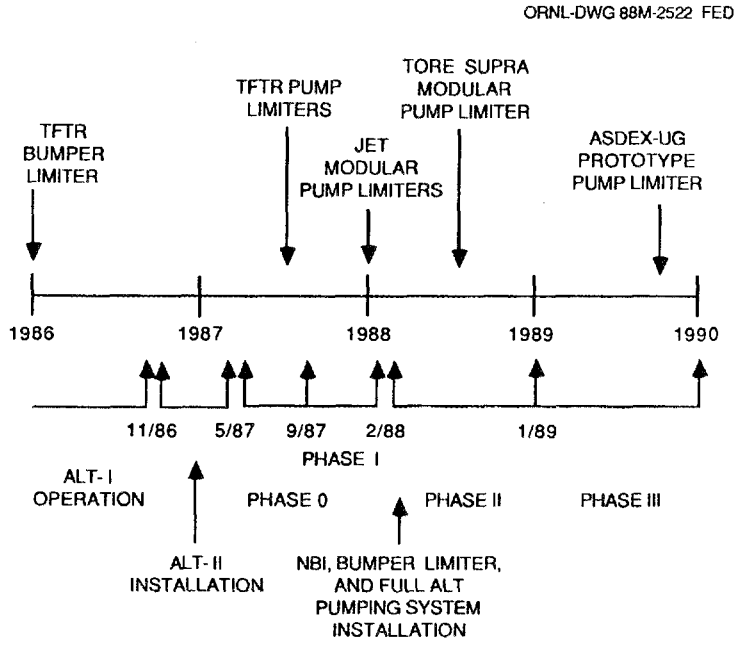

Fig. 1. ALT-II experimental program outline. Schedules for belt limiter and modular pump limiter experiments on other large tokamaks are shown for comparison.

Table 1. Typical core and edge plasma parameters in TEXTOR

Magnetic field B, T	2
Plasma current I_p, kA	350–450
Discharge duration, s	3–4
Plasma current flattop duration, s	1.5
n_e, cm^{-3}	
Edge	$1\text{–}2 \times 10^{12}$
Core	$\leq 5 \times 10^{13}$
T_e, eV	
Edge	20–40
Core	800–1200
Edge density scale length λ_Γ, cm	~ 1

In Sect. II, we discuss the ALT-II pump limiter system and its basic parameters. In Sect. III, the layout and characteristics of the H_α monitor are given. In Sect. IV, we develop a model for estimating the particle fluxes from the measurements of the H_α radiance. The absolute calibration of the monitors is covered in Sect. V. In Sect. VI, we discuss the use of the monitor results for assessing the ALT-II performance, recycling, and particle balance and for estimating the particle confinement time. In Sect. VII, the locations of the initial-phase monitors on TEXTOR are given. The results obtained during the initial-phase ALT-II experiments, during which the limiter blades were inserted to $r = 46$ cm from their resting position of 48.5 cm, are presented in Sect. VIII. The particle fluxes in the core plasma and on the wall and the limiter are estimated, and the global confinement time is calculated for the stationary part of the plasma discharge. General remarks and discussions are contained in Sect. IX.

II. ALT-II PUMP LIMITER SYSTEM

The ALT-II toroidal belt pump limiter is an extension of the ALT-I modular pump limiter previously operated on TEXTOR. The ALT-II limiter consists of eight blade segments, each about 28 cm wide and 1.7 cm thick, covered by graphite tiles mounted on adjustable supports (movable over about 5 cm radially) located 45° below the outboard midplane of the device, as shown in Fig. 2. A 45° neutralizer plate behind each blade looks to a pumping chamber. The resting location of the ALT-II is 48.5 cm. The nominal operating location of the ALT-II is $a_\ell = 46$ cm; in this position it is the main limiter of the system. Experiments are also planned with ALT-II located at 44 cm. The basic objective of this pump limiter is to demonstrate plasma density and impurity control during long-pulse (about 4-s) operation of the TEXTOR tokamak in the presence of neutral beam injection (NBI) and ICH (total auxiliary power of about 5 MW). The pump limiter system is designed to remove 5 to 10% of the plasma efflux with a minimum pumping capacity of 30–40 m^3/s. The limiter can withstand heat loads up to 300 W/cm^2, which is the maximum heat flux for which the leading edges of the blades are contoured.

III. H_α MONITOR LAYOUT

A schematic of the H_α monitor and its components is shown in Fig. 3. Basically, a narrow band ($\Delta\lambda = 10$ nm) interference filter is used to obtain the H_α radiation

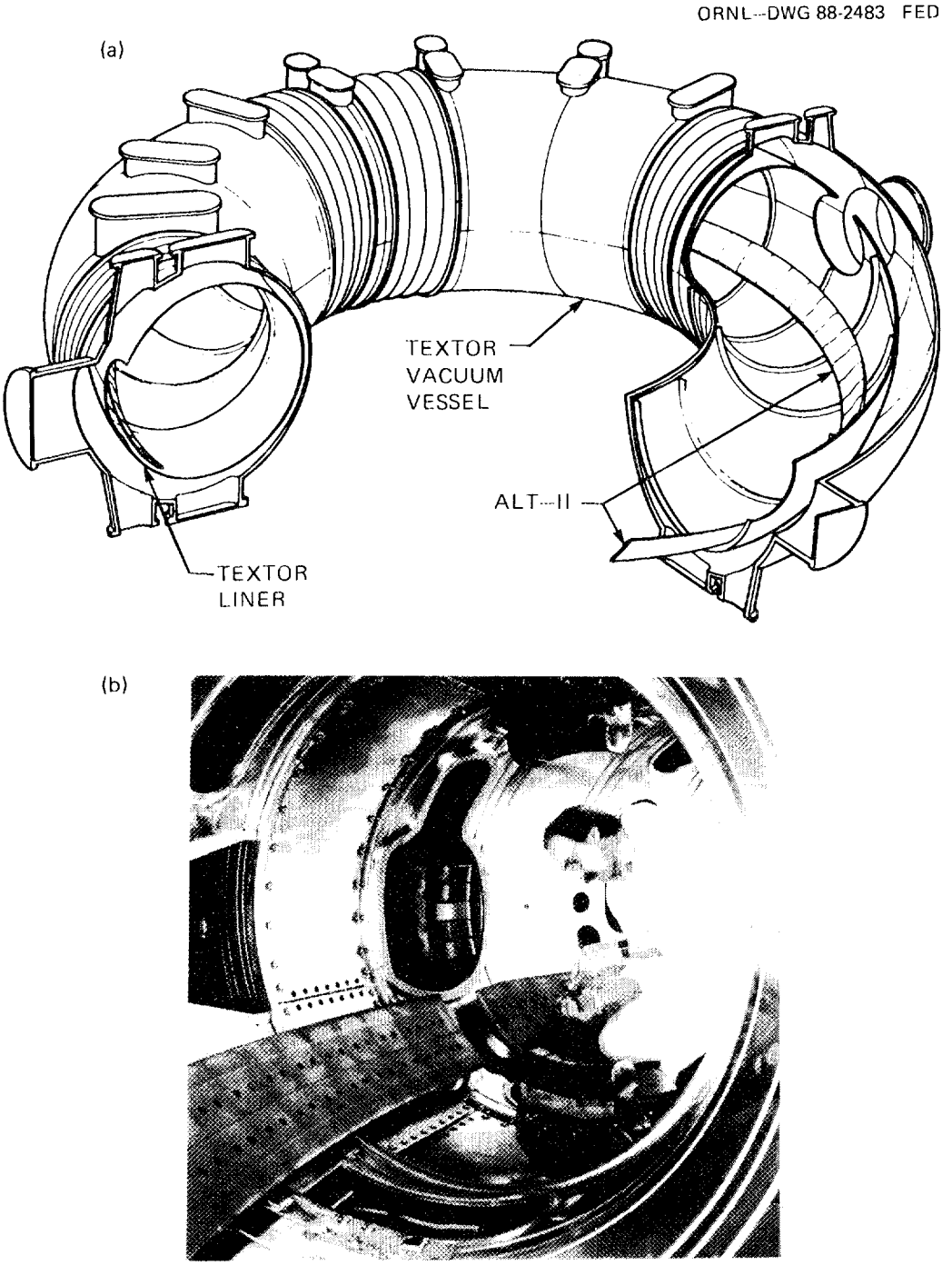

Fig. 2. (a) Cutaway view of ALT-II toroidal belt pump limiter on TEXTOR. (b) Photograph of the inside of the vacuum vessel, showing ALT-II and the poloidal sections of the main limiter.

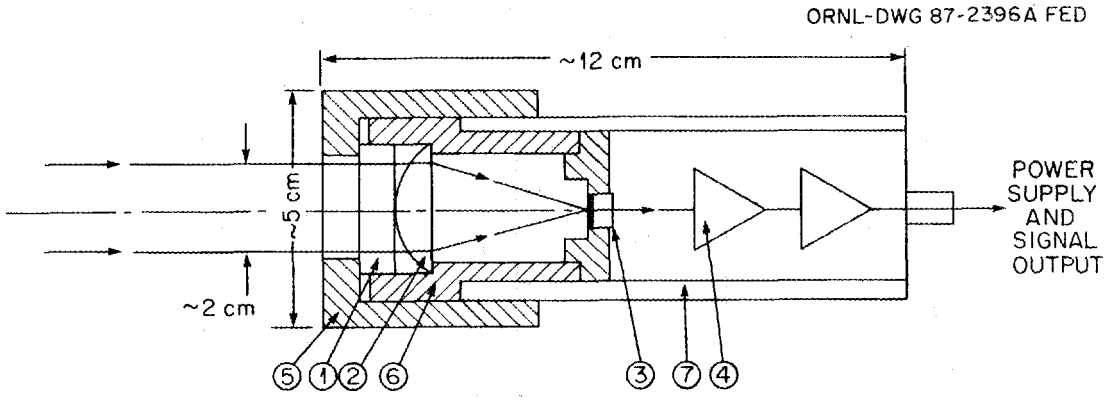

- Components of the H_α monitor are:
  1. Narrow band interference filter, 656 nm
  2. Plano-convex spherical lens, 26.5 mm
  3. Photodiode, active area 5.1 mm^2
  4. Signal amplifier (PS: $\mp$ 15 V_{DC})
  5. Micarta for isolation
  6. Black plastic, cuts reflections
  7. Aluminum pipe
- Bandwidth: DC-5 kHz
- Output voltage: 0-15 V

Fig. 3. Schematic view of the H_α monitor on TEXTOR.

($\lambda_{H_\alpha} = 653$ nm). The light is focused on a photodiode for detection, and the signal is amplified. Figure 4 shows the response function of the filter used. The photodiode has an effective area of 5.1 cm^2; its characteristic response is presented in Fig. 5. Details of the photodiode's characteristics and its operation are given in Ref. 6. The diameter of the detector aperture is $D = 19$ mm, which can be reduced if the detector saturates. The field of view of the detector is 5.5°, and it has a maximum light throughput of $(A\Omega)_d = 2.07 \times 10^{-2}$ sr·cm^2. The monitor output voltage V_{out} is linear with the light input up to 15 V, and the bandwidth is about 5 kHz.

Figure 6 is a simplified electrical equivalent circuit diagram of the monitor. The circuit consists of a photodiode and two high-gain operational amplifiers. This model is very helpful in estimating the calibration factors of the monitors during design, as discussed in Sect. V.

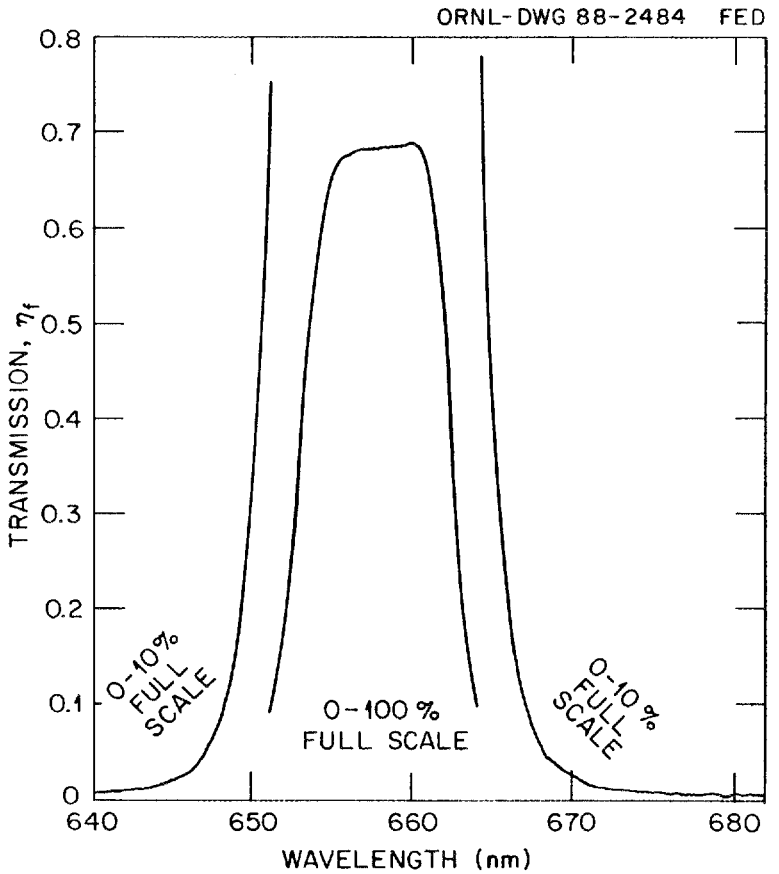

Fig. 4. Response function of the interference filter of the H_α monitor.

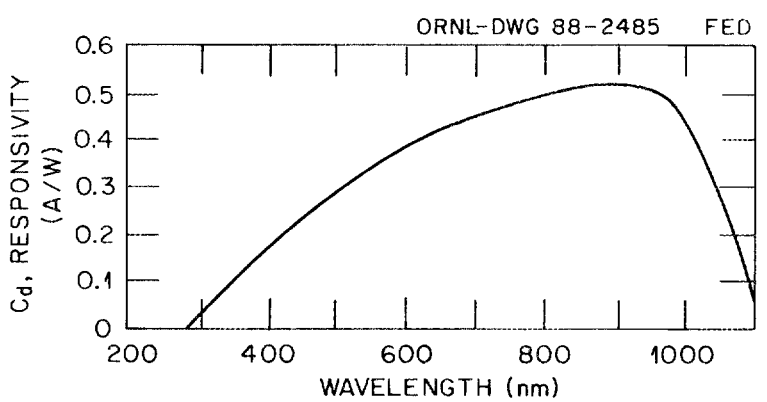

Fig. 5. Response function of the photodiode of the H_α monitor.

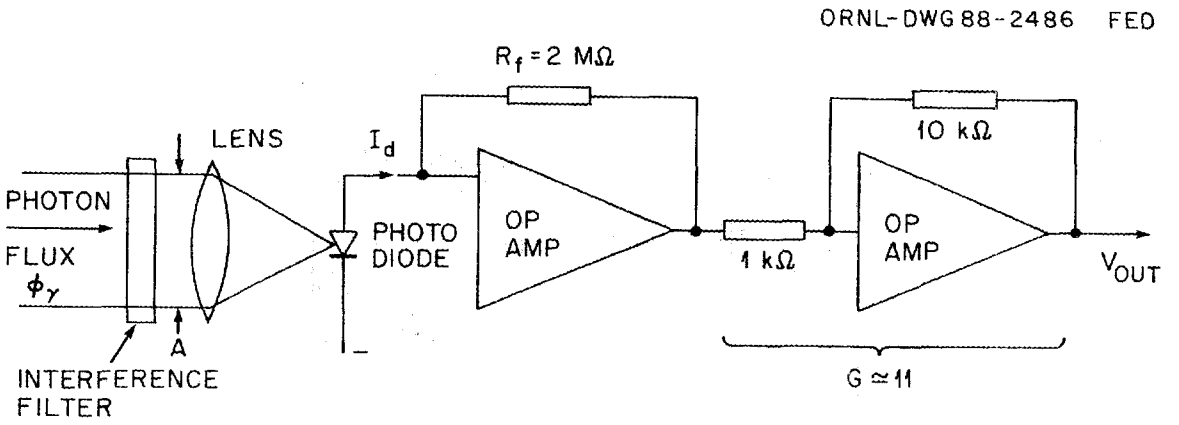

Fig. 6. Schematic of the monitor electrical circuitry.

A number of tests and checks were performed after the detectors were installed on TEXTOR: measurements of signal-to-noise ratio, thermal drift and reproducibility, reliability, and signal levels at various plasma densities. The results were very satisfactory. For example, the thermal drift of the monitor during 4 h of operation is shown in Fig. 7(a); no apparent drift is observed. The monitor noise level, displayed in Fig. 7(b), is only the bit noise (~2.5 mV) of the data sampling system. The detectors performed very well in every phase of the measurements and experiments.

A typical H_α signal from one of the monitors, together with plasma density during the TEXTOR discharge, is shown in Fig. 8. The H_α signal, Fig. 8(a), almost follows the density except in the early phase of the discharge, when there is a finite gas injection during the first ~0.25 s, as shown in Fig. 8(b), and the H_α emission is considerably higher during the gas breakdown.

IV. MODEL FOR ESTIMATING PARTICLE FLUX

Although the H_α emission is being modeled[7] with the DEGAS neutral transport code,[8] it is useful to make first-order estimates of the particle fluxes from the measurements of the H_α radiance. To do so, we need to relate the measured H_α radiance (signal), N_γ, to the edge plasma particle fluxes. In this discussion we assume that a hydrogen (or deuterium) atom leaving the wall or limiter enters the edge plasma, where it is excited by collisions with electrons. As a result, it gives off H_α radiation, $H^0 + e^- \rightarrow e^- + H^*$ (Balmer alpha radiation). Similar radiation can also occur

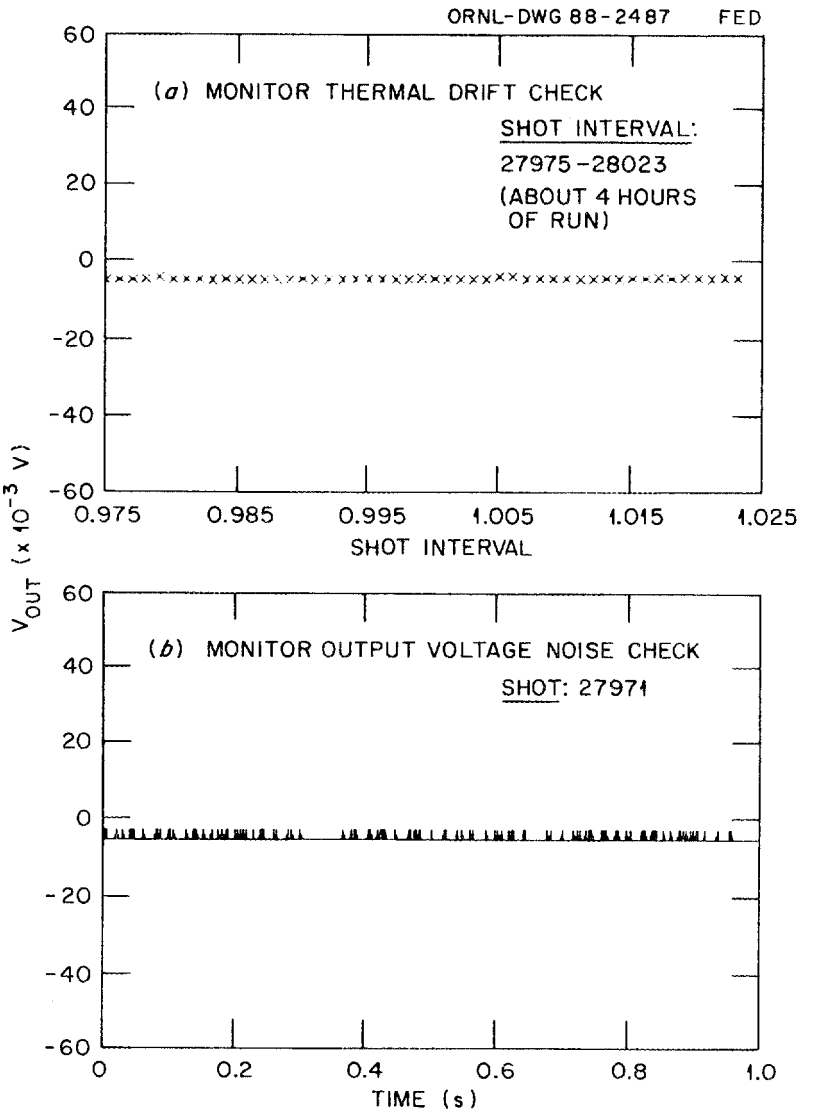

Fig. 7. (a) Absence of thermal drift during 4 h of operation. (b) Absence of monitor output noise. The noise in the figure is the bit noise (2.4 mV) of the data acquisition system.

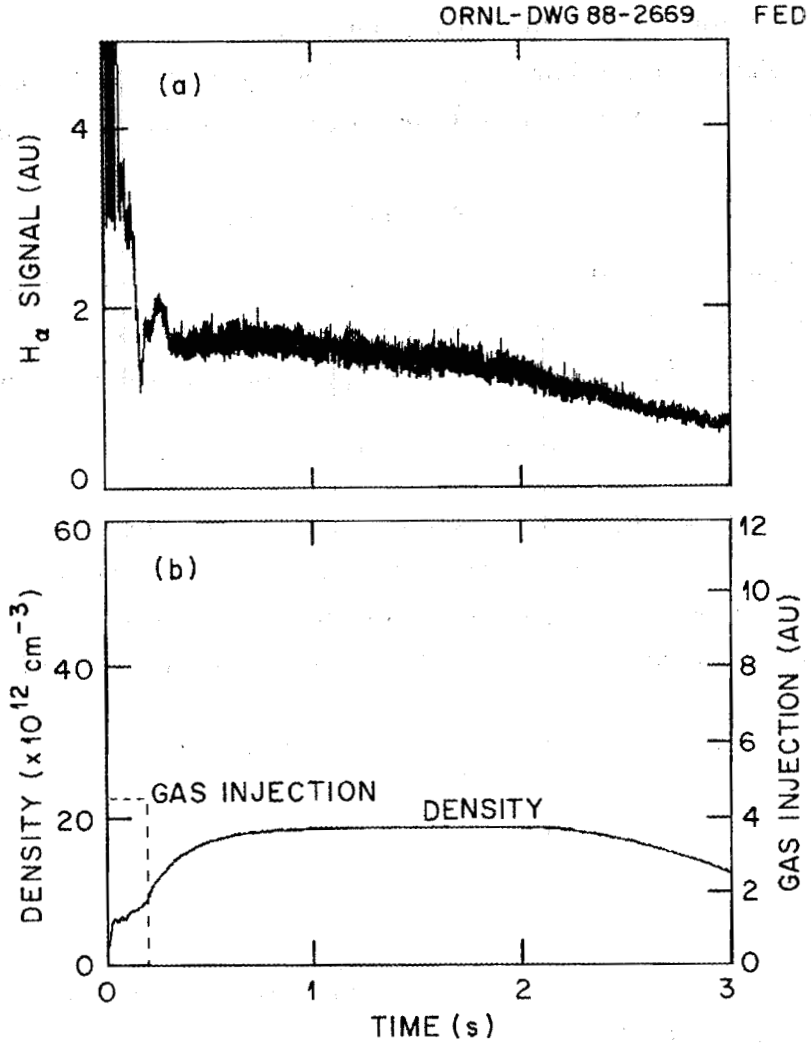

Fig. 8. (a) A typical H_α signal from one of the monitors and (b) measured plasma density during the TEXTOR discharge. The H_α signal in (a) almost follows the plasma density except in the early phase of the discharge, during which there is a finite gas injection for the first ~0.25 s, as shown in (b); the H_α signal is considerably higher during this gas breakdown.

from the dissociation of molecular hydrogen, but the cross-section ratio of these two processes is $\sigma_{\rm exc}/\sigma_{\rm diss} \approx 5$ for edge plasma temperatures of $T_e = 20$–40 eV, which are typical for TEXTOR. Therefore, for this study we consider only excitation of the atomic hydrogen as a source of H_α radiation.

For simplicity, we consider a one-dimensional geometry for the plasma edge: the slab model shown in Fig. 9. The H_α emission rate density for a unit area is given by[9]

$$dN_\gamma/dx = (1/4\pi)n_3 A_{32} \ , \tag{1}$$

where N_γ has units of photon·sr^{-1}·s^{-1}·cm^{-2}, n_3 is the population density of the $n = 3$ level in neutral hydrogen, and A_{32} is the transition probability to the $n = 2$ state as shown in Fig. 10. From the assumption of corona excitation,[9] we write

$$n_e n_1 \langle \sigma v_e \rangle_{\rm exc} = n_3 (A_{13} + A_{23}) \ , \tag{2}$$

where $n_1 \equiv n_0(x)$ and $n_e(x)$, which are the neutral atom and electron local densities, respectively; $\langle \sigma v_e \rangle_{\rm exc}$ is the collisional electron excitation rate for the upper level of the transition; and the A_{ij} are the transition probabilities of the excited atom's energy states, as depicted in Fig. 10. Using Eq. (2) in Eq. (1), we find

$$N_\gamma = (B/4\pi) \int_0^x dx \ n_0(x) n_e(x) \langle \sigma v_e \rangle_{\rm exc} \ , \tag{3}$$

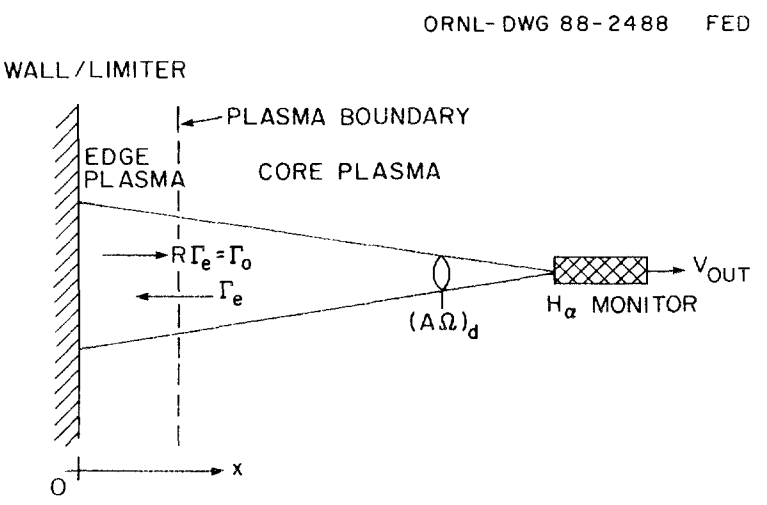

Fig. 9. Slab model of the plasma edge that is viewed by a H_α monitor.

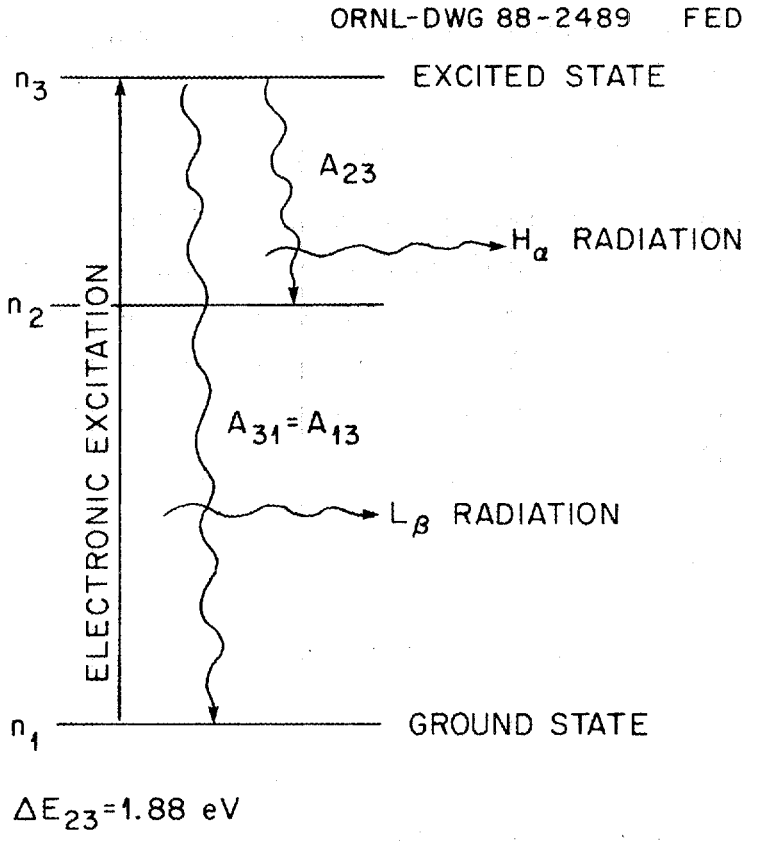

Fig. 10. Energy states of the atomic hydrogen and the H_α radiation from the excited state.

where B is the branching ratio, $B \equiv A_{32}/(A_{31} + A_{32})$, and is typically $B = 0.5$ for the Balmer alpha radiation.[10] The particle flux that is leaving the plasma edge can be calculated by integrating the continuity equation,

$$\Gamma_e = -\int_0^x dx\ n_0 n_e \langle \sigma v_e \rangle_{\rm ion}\ , \tag{4}$$

where $\langle \sigma v_e \rangle_{\rm ion}$ is the ionization rate coefficient. Considering the particle recycling from the wall/limiter, we obtain the neutral particle flux,

$$\Gamma_o = R\Gamma_e = \int_0^x dx\ n_0 n_e \langle \sigma v_e \rangle_{\rm ion}\ , \tag{5}$$

where R is the global recycling coefficient of the wall/limiter and in this case $R = -1$. By comparing Eqs. (3) and (5), we get

$$\Gamma_o = (\langle \sigma v_e \rangle_{\rm ion} / \langle \sigma v_e \rangle_{\rm exc})(4\pi/B) N_\gamma\ . \tag{6}$$

Here Γ_o represents the neutral particle flux from the wall/liner or the limiter. We may rewrite Eq. (5) as

$$C_o \equiv \Gamma_o/N_\gamma = (\langle\sigma v_e\rangle_{\rm ion}/\langle\sigma v_e\rangle_{\rm exc})(4\pi/B) \ . \tag{7}$$

This factor C_o, which has units of particle·sr·photon^{-1}, clearly depends on the edge plasma temperature and should be estimated to allow calculation of the particle fluxes from the H_α measurements. For example, in Fig. 11, we display C_o for T_e = 20–60 eV, the typical TEXTOR edge plasma temperature.[4] For a H_α monitor that is looking to the wall/limiter, the output signal is related to the total photon flux received; that is,

$$\phi_\gamma = C_\gamma V_{\rm out} = (A\Omega)_d N_\gamma \ . \tag{8}$$

Using Eq. (7), we get

$$\Gamma_o = [C_\gamma C_o/(A\Omega)_d]V_{\rm out} = C_{\rm flux} V_{\rm out} \ , \tag{9}$$

where

$$C_{\rm flux} \equiv [C_\gamma C_o/(A\Omega)_d] \tag{10}$$

and C_γ is the absolute H_α light calibration factor of the monitor, which is discussed in detail in Sect. V.

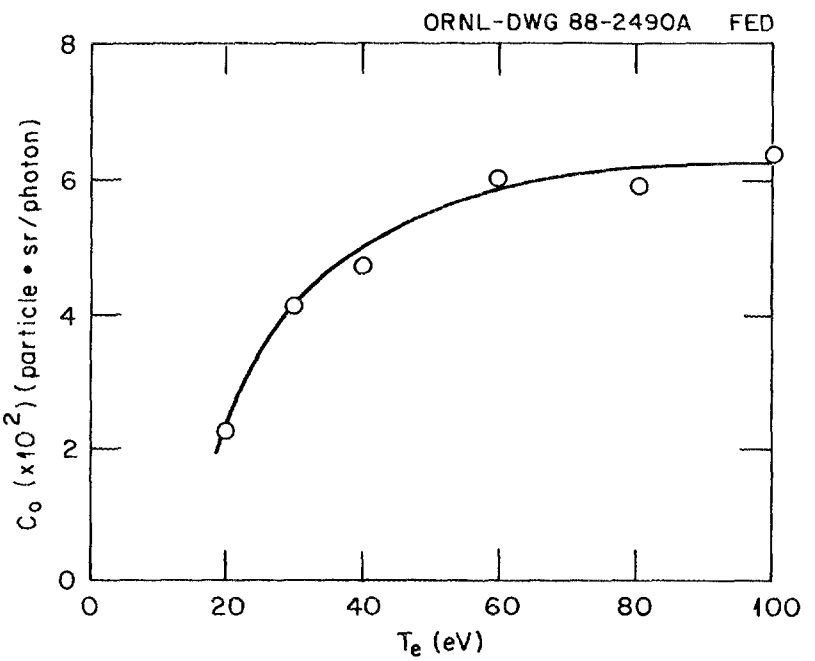

Fig. 11. Variation of $C_o \equiv \Gamma_o/N_\gamma$, Eq. (7), with T_e.

V. MONITOR CALIBRATION

In order to estimate the particle flux from the H_α measurement, the monitors are absolutely calibrated with a standard light source, in this case a tungsten halogen lamp made by EG&G.[11] The light source is chopped at 100 Hz to prevent saturation of the monitor output during this process, as required by the monitor's electrical circuit design. The monitor is placed 200 cm away from the source with its aperture reduced to 0.5 cm in diameter. The voltage output V_{out} of the monitor is recorded on a storage scope as a function of the known photon energy flux ϕ_γ received. Table 2 presents the calibration results, $C_\gamma = \phi_\gamma / V_{out}$, for the monitors and their specific locations on TEXTOR.

As we see from Fig. 6, when the monitor is illuminated by a light source with a known spectral irradiation, P_{in} (W/cm^2·nm) at the wavelength $\lambda_{H_\alpha} = 653$ nm, on the lens, the detector's photodiode current I_d depends only on this photon energy flux as received within the bandwidth of the interference filter and the detector aperture area A. One H_α photon has an energy of 1.88 eV, as shown in Fig. 10; thus, we have

$$\phi_\gamma = 3.325 \times 10^{18} P_{in} \Delta\lambda A \ . \tag{11}$$

Table 2. Locations and calibration factors of TEXTOR H_α monitors

Monitor number	Location	Aperture diameter (cm)	C_γ (photon·s^{-1}·V) (10^{11})	C_{flux} (cm^{-2}·s^{-1}·V^{-1}) (10^{16})
HA1	ICH antenna 1	10	6.9	4.8
HA2	Vertical observation	19	6.32	1.2
HA3	ALT-II blade/ limiter	10	6.6	4.6
HA4	Wall/liner	19	6.06	1.2
HA5	ALT-II blade tip	13	6.25	2.6
HA6	ICH antenna 2	10	6.06	4.2

From the transmission factors of the lens, η_l, and the filter, η_f, and the response function of the photodiode $C_d(\lambda_{H_\alpha})$, as shown in Fig. 5, we can express the output voltage of the detector as

$$V_{out} = I_d R_f G = (P_{in} \Delta\lambda A C_d \eta_l \eta_f) R_f G \ , \tag{12}$$

where R_f is the feedback resistance of the input circuit and G is the voltage gain of the following stage. Using Eqs. (11) and (12) in the definition of the calibration factor, Eq. (8), we find

$$C_\gamma = (3.325 \times 10^{18})/(R_f G C_d \eta_l \eta_f) \ . \tag{13}$$

The monitor design parameters are as follows:

$R_f = 2$ MΩ,
$G = 11$,
$C_d(\lambda_{H_\alpha}) = 0.42$ A/W,
$\eta_l = 92\%$,
$\eta_f = 62\%$.

Using these parameters in Eq. (13), we obtain

$$C_\gamma = 6.3 \times 10^{11} \text{ photon/s} \cdot \text{V} \ . \tag{14}$$

We see from Table 2 that this value is about what we have measured experimentally for the monitors.

Equation (13) is also particularly useful in the design of the monitors. If the expected particle flux can be estimated, then the required R_f and G can be calculated for a desired value of the detector output voltage, which may be determined from the requirements of the available data acquisition system.

We can relate the monitor output signal to the plasma flux in which we are interested by using the model that we discussed in conjunction with the detector calibration. When we install the monitor on the device, it will collect light through the plasma column emanating from the far side (FS) as well as from the near side (NS) of its field of view. This is as a result of the short mean free path ($\leq$10 cm for the TEXTOR plasma parameters) of the neutral particles at the edge that create an annulus light source at the plasma periphery, as observed with a spatial television camera on TEXTOR. Therefore, the total photon flux received by the detector is actually

$$\phi_\gamma = C_\gamma V_{out} = [N_\gamma(\text{FS}) + N_\gamma(\text{NS})](A\Omega)_d \ , \tag{15}$$

and using Eq. (7) in Eq. (15), we write

$$\Gamma_o(\mathrm{FS}) + \Gamma_o(\mathrm{NS})[C_o(\mathrm{FS})/C_o(\mathrm{NS})] = [C_\gamma C_o(\mathrm{FS})/(A\Omega)_d]V_{\mathrm{out}} \ . \tag{16}$$

Furthermore, if we assume poloidal symmetry in the edge plasma temperature, so that $C_o(\mathrm{FS})/C_o(\mathrm{NS}) \sim 1$, then Eq. (16) becomes

$$\Gamma_o(\mathrm{FS}) + \Gamma_o(\mathrm{NS}) = C_{\mathrm{flux}} V_{\mathrm{out}} \ . \tag{17}$$

Here again

$$C_{\mathrm{flux}} = C_\gamma C_o(\mathrm{FS})/(A\Omega)_d \ , \tag{18}$$

As a typical case, if we take $T_e = 25$–30 eV for the edge plasma, with C_γ from Eq. (12), for a full-aperture monitor, $D = 19$ mm, then

$$C_{\mathrm{flux}} = 1.2 \times 10^{16} \ \mathrm{cm}^{-2} \cdot \mathrm{s}^{-1} \cdot \mathrm{V}^{-1} \ . \tag{19}$$

This factor may be modified if the monitor aperture must be reduced to keep the voltage output from saturating. For example, as we see later, on TEXTOR the blade monitor aperture was reduced to $D_{\mathrm{L}} = 10$ mm.

VI. MEASUREMENT PARAMETERS ON TEXTOR

In this study, we are interested only in the case in which the ALT-II is the main limiter of TEXTOR, which happens when it is at $r = a_\ell = 46$ cm. The H_α measurements obtained from the wall/liner monitor are simply related to the wall/liner radial flux $\Gamma_o(\mathrm{w})/R$. The limiter blade flux $\Gamma_o(\mathrm{L})$ obtained from the limiter blade monitor, on the other hand, can be related to the poloidal edge flux $\Gamma_\theta(x = 0)$ that hits the blade leading edge, and the resulting emitted neutral particle flux may obey a cosine distribution. In this case, considering the geometry and the angle of field of view of the blade monitor with respect to the vertical direction, we write

$$\Gamma_o(\mathrm{L}) \approx R\Gamma_\theta \cos(2\alpha + \theta_{\mathrm{L}}) \ , \tag{20}$$

where θ_{L} is the poloidal angle of the limiter location, which is 45° for ALT-II, and α is the shaped angle of the blade leading edge, which is about 10°, as illustrated schematically in Fig. 12. Here we ignore the contribution from the radial core flux on $\Gamma_o(\mathrm{L})$, since typically (core flux/poloidal flux) $\sim 10^{-3}$–10^{-2}.

We now discuss how we can use these measured fluxes to study the performance of ALT-II and the particle balance considerations in TEXTOR.

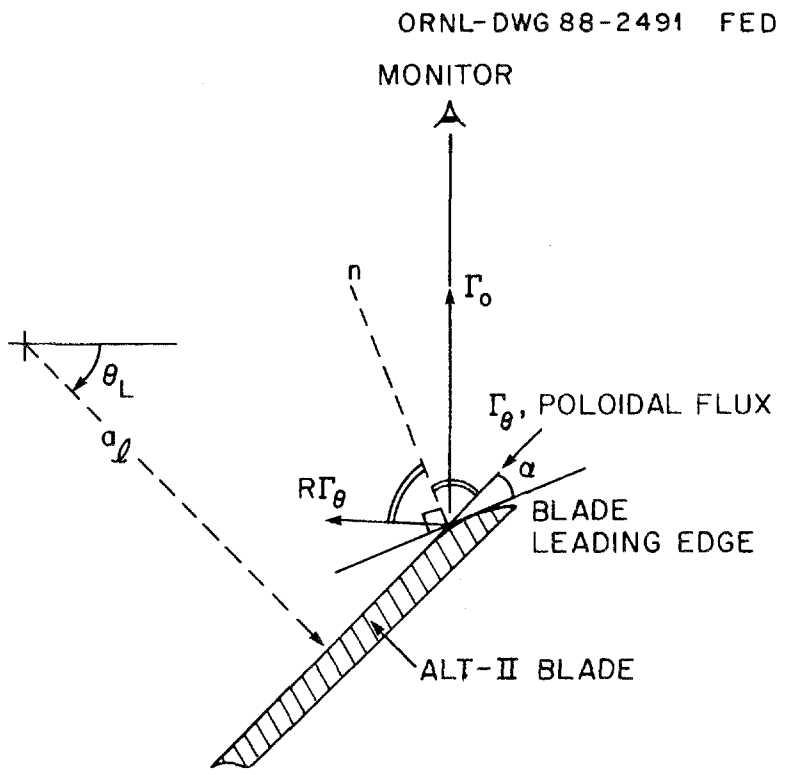

Fig. 12. Schematic of the ALT-II leading edge used for obtaining Eq. (20).

A. ALT-II Performance Studies

One performance parameter for ALT-II is the exhaust efficiency ϵ, which indicates the fraction of the total particle efflux N_e/τ_p that is pumped out of the system:

$$\epsilon = p_0 S_{\rm eff}/(N_e/\tau_p) \ , \tag{21}$$

where N_e is the total core plasma density and τ_p is the global particle confinement time. The particle exhaust is estimated from the pressure buildup p_0 in the pumping chamber and the effective pumping speed $S_{\rm eff}$ as $p_0 S_{\rm eff}$. Therefore, to assess the operation of the ALT-II, we need to know N_e/τ_p, which can be related to the total particle fluxes from the edge. As we have discussed, the absolute value of the total H_α radiance from the edge represents the measure of the total recycled particles ϕ_o from the wall/liner, ϕ_w, or the limiter, ϕ_L. Namely,

$$\phi_o = R\phi_\perp \ , \tag{22}$$

where $\phi_\perp = N_e/\tau_p$ is the total particle efflux and

$$\phi_o = \Sigma_j \phi_j = \phi_w + \phi_L \ . \tag{23}$$

Here, knowing the area of the wall and the effective limiter area, we write

$$\phi_w = \int dA \ \Gamma_o|_{wall}$$

and

$$\phi_L = \int dA \ \Gamma_o|_{limiters} \ .$$

In general, Γ_o may have a poloidal (θ) and toroidal (φ) dependence. Therefore, a number of H_α monitors are placed around the device to obtain $\Gamma_o(\theta, \varphi)$. In addition to the limiters, a possible source of particle recycling is the presence of ICH antennas at the edge; TEXTOR has two antennas.

B. Particle Balance Studies and Recycling

To study particle confinement in the device, we need to understand the particle recycling mechanism through the edge particle fluxes in various operating modes of the device. To do this, we start with the particle balance equation

$$dN_e/dt = \phi_{ext} + (R-1)N_e/\tau_p \ , \tag{24}$$

where ϕ_{ext} is the external fueling source (i.e., gas puff, pellet injection, NBI, and their respective fueling efficiencies must be considered) and R, as noted, represents the global particle recycling coefficient. Here N_e/τ_p is related to the total radiance of H_α as

$$\phi_o = R(N_e/\tau_p) \ ; \tag{25}$$

also, ϕ_o is related to the total ionization source at the edge; that is, $\sum_j \phi_j = \phi_o$. Using Eq. (25) in Eq. (24), we get

$$R = \phi_o/[\phi_{ext} + \phi_o - (dN_e/dt)] \ . \tag{26}$$

The effect of the ALT-II pump limiter on recycling can be investigated through Eq. (26). For example, in the case of $\phi_{ext} = 0$, we can estimate R simply by simultaneously measuring the density decay, $\tau_p^* = (-dN_e/dt)^{-1} N_e$, and the total H_α radiance when the ALT-II pumps are turned on.

C. Global Particle Confinement Time

The global particle confinement, or replacement, time can be estimated from

$$\tau_p = N_e/\phi_\perp = RN_e/\phi_o \ , \tag{27}$$

where

$$\phi_\perp(x=0) = (\phi_w + \phi_L)/R = a_\ell R_0 \int_0^{2\pi} d\theta \int_0^{2\pi} d\varphi \ \Gamma_\perp(x=0,\theta,\varphi) \ , \tag{28}$$

which is the total radial flux passing through the plasma boundary, $x = 0$ (or $r = a_\ell$), whose area is $A_\perp(x=0) = 4\pi^2 a_\ell R_0$, as shown in Fig. 13. Here the

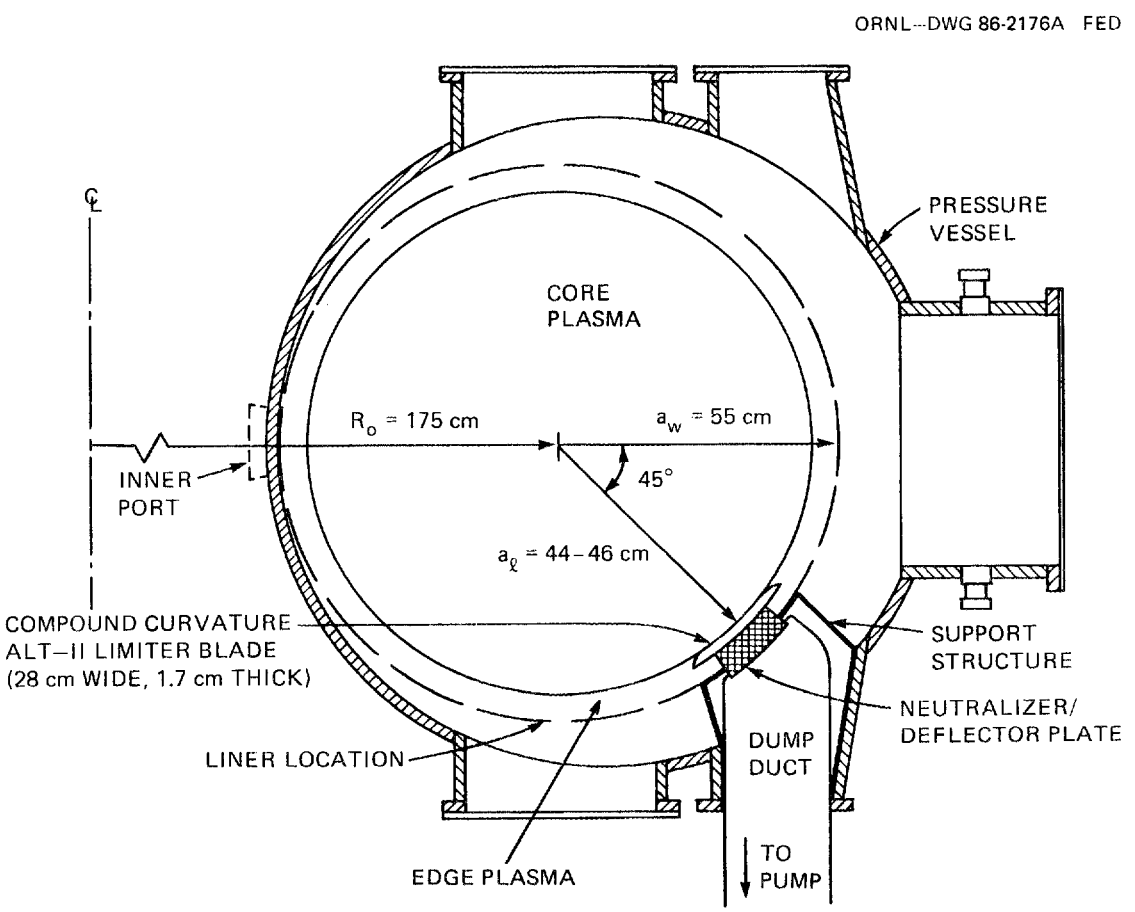

Fig. 13. Cross section of the TEXTOR vacuum vessel, showing ALT-II and the core and edge plasmas.

recycling coefficient may be obtained from Eq. (26). For the sake of making a first-order estimate of τ_p, if we ignore the θ and φ dependences of the radial edge flux $\Gamma_\perp$, then Eq. (28) simply becomes

$$\phi_\perp(x=0) = A_\perp \Gamma_\perp(x=0) \ . \tag{29}$$

Moreover, if we ignore the source term in the continuity equation (for example, by staying far enough from the limiter), then we have the relation between $\Gamma_\perp$ and the parallel flux along the magnetic field line $\Gamma_\parallel$ and the wall/liner flux $\Gamma_o(\mathrm{w})$ within the flux tube defined by the limiter,

$$\Gamma_\perp = \Gamma_o(\mathrm{w}) + (\lambda_\Gamma / L_c)\Gamma_\parallel \ , \tag{30}$$

where λ_Γ represents the characteristic scale length of the edge flux and

$$L_c = \pi q R_0 \tag{31}$$

is the connection length for the ALT-II toroidal belt limiter. We can also relate $\Gamma_\parallel$ to Γ_θ as follows:

$$\Gamma_\parallel = \Gamma_\theta (q R_0 / a_\ell) \ . \tag{32}$$

In terms of the ion sound speed c_s, the particle flux along the magnetic field line may be calculated from[12]

$$\Gamma_\parallel = v_\parallel n_e(x=0) = 0.3 n_e c_s \ , \tag{33}$$

which can be obtained from measurements of the edge plasma density $n_e(x=0)$ and the temperature $T_e(x=0)$.

The cross-field diffusion coefficient $D_\perp$ of the boundary may be calculated from the radial edge flux $\Gamma_\perp(x=0)$ and from the measurements of the characteristic density scale length λ_n of the edge as

$$D_\perp = \Gamma_\perp(x=0)[\lambda_n / n_e(x=0)] \ . \tag{34}$$

Finally, by combining Eqs. (26) and (27) we can estimate the global particle confinement time from the measured total H_α radiance and density as follows:

$$\tau_p = \tau_p^* / [1 + (\phi_{ext} + \phi_o)(\tau_p^* / N_e)] \ . \tag{35}$$

For example, if only gas injection is present, then $\phi_{ext} = \phi_{gas}\eta_{fueling}$, where ϕ_{gas} is the gas injection rate and $\eta_{fueling}$ is the fueling efficiency ($\sim$50–100%).

In Sect. VIII, we use these relations and the experimental measurements made with the H_α monitors on TEXTOR to estimate the various edge fluxes.

VII. MONITOR LOCATIONS ON TEXTOR

Measurements of the H_α emission were performed in TEXTOR following the recent installation of ALT-II. These measurements are carried out to determine the distribution of particle fluxes in the plasma vessel as a function of location, time, plasma parameters, and heating method. Our main goal is to study recycling and global particle confinement and their correlation to plasma performance with the ALT-II toroidal belt pump limiter, but we are also interested in the core plasma confinement characteristics resulting from the recycling control. For this purpose, initial-phase, absolutely calibrated H_α monitors are distributed around the device to measure the toroidal and poloidal variations of the particle fluxes, particularly in the regions near the ALT-II limiter blade and tip, on the vacuum vessel liner, and on both ICH antennas. One monitor is placed to make vertical observations of the plasma cross section. The locations of the monitors are shown in Fig. 14. The field of view of each monitor is illustrated in Fig. 15. Up to nine monitors are planned; areas to be observed include the future inner bumper limiter, NBI, and the device gas puff. The total number of monitors may change as warranted by the information obtained in the various phases of the ALT-II experiments.

VIII. EXPERIMENTAL OBSERVATIONS AND RESULTS

Before we discuss the experimental observations, let us briefly review how we calculate the wall/liner flux $\Gamma_o(\mathrm{w})$ and the ALT-II limiter blade flux $\Gamma_o(\mathrm{L})$ from the monitors that look vertically through the plasma cross section, as shown in Fig. 16. Here $V_{\mathrm{out}}(\mathrm{w})$ is the output voltage from the monitor $H_\alpha(\mathrm{w})$ that views the TEXTOR vacuum vessel wall/liner, and $V_{\mathrm{out}}(\mathrm{L})$ is the output voltage from the monitor $H_\alpha(\mathrm{L})$ that views the blade. Since the viewing cross section of $H_\alpha(\mathrm{w})$ is far enough from the limiter blade, which is the particle source, we may assume $\Gamma_o(\mathrm{FS}) \sim \Gamma_o(\mathrm{NS})$ for the wall fluxes. Thus, from Eq. (17), we write

$$\Gamma_o(\mathrm{w}) = 0.5 C_{\mathrm{flux}}(\mathrm{w}) V_{\mathrm{out}}(\mathrm{w}) \ . \tag{36}$$

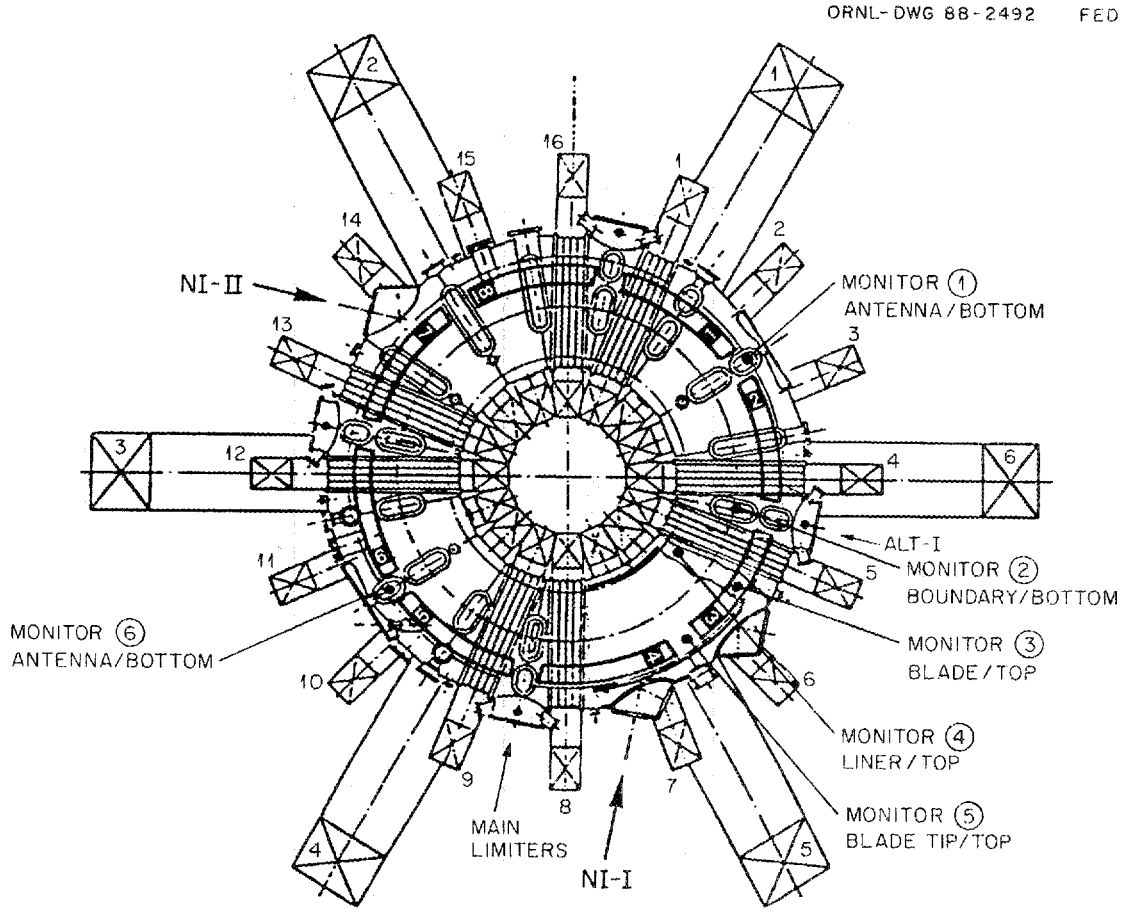

Fig. 14. Top view of the TEXTOR tokamak showing the locations of the monitors. Here the ALT-II blades are numbered from 1 through 8.

On the other hand, $H_\alpha(L)$ observes $\Gamma_o(w) + \Gamma_o(L)$; hence

$$\Gamma_o(L) = C_{flux}(L)V_{out}(L) - \Gamma_o(w) \ . \tag{37}$$

Here $C_{flux}(w)$ and $C_{flux}(L)$ are the flux calibration factors of the wall and the limiter monitors, respectively.

Let us now discuss the H_α measurement results obtained during the initial-phase ALT-II experiments, during which the blades were moved, one at a time, to $r = a_\ell = 46$ cm from their resting position of $a_s = 48.5$ cm. In Fig. 17 we display plasma shots for which the line-averaged core plasma density was kept constant ($n_e = 2.5 \times 10^{13}$ cm^{-3}) while the blades were inserted. For these experiments no

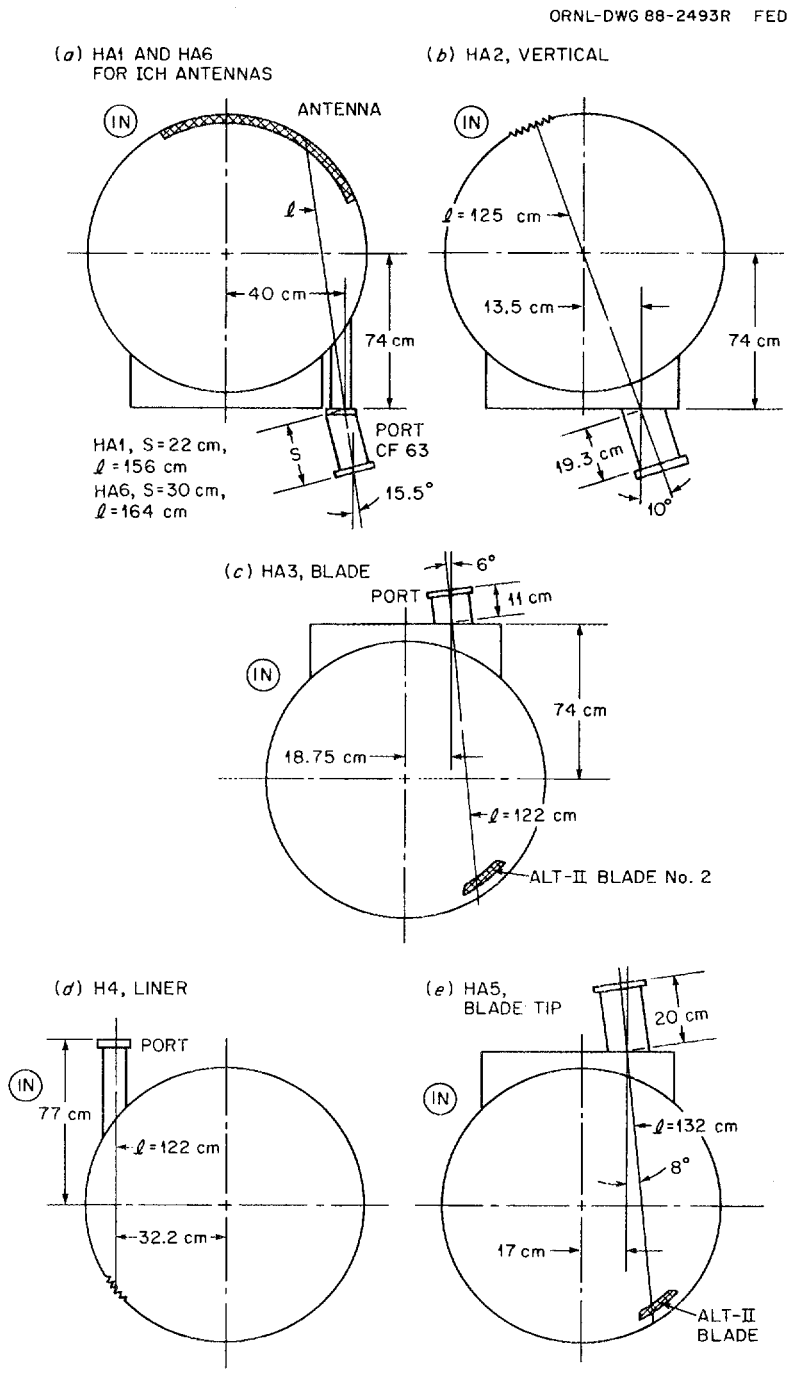

Fig. 15. Schematic of the fields of view of the monitors for (a) ICH antennas 1 and 2, (b) vertical plasma observation, (c) ALT-II blade 2, (d) wall/liner, and (e) blade tip. Here ℓ represents the length of the viewing chord.

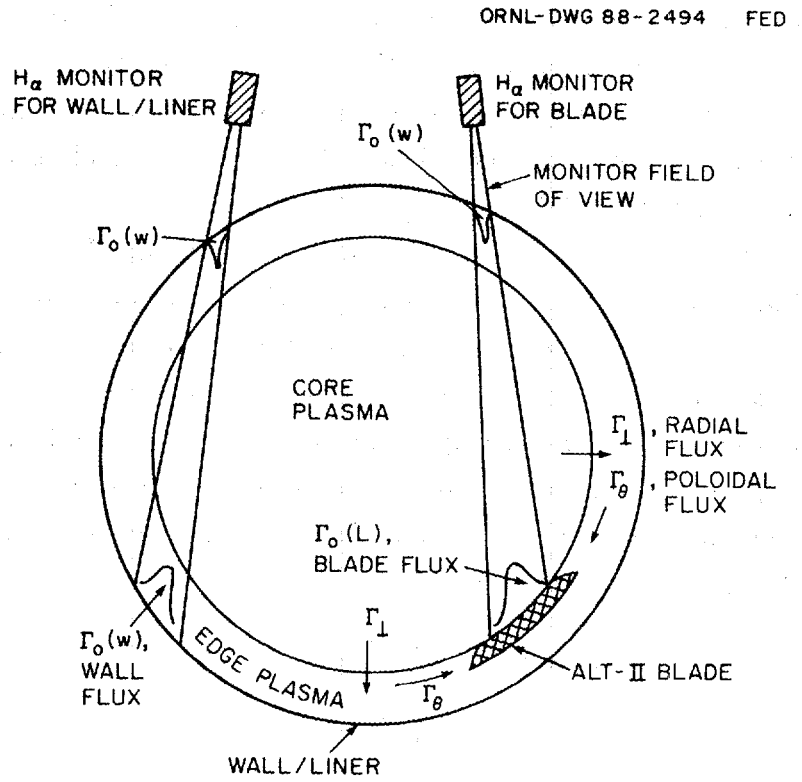

Fig. 16. Schematic plasma cross section with the wall/liner and the blade/limiter monitors.

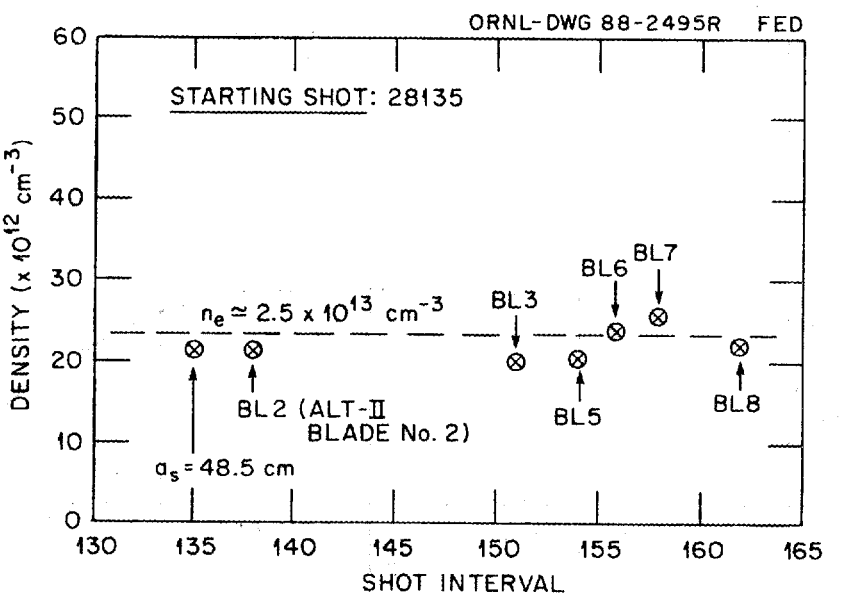

Fig. 17. ALT-II experimental shots with constant density.

external gas is used during the discharges (i.e., $\phi_{ext} = 0$). The typical plasma density during one of the discharges is shown in Fig. 18. The measured voltage output $V_{out}(L)$ of the limiter monitor as the ALT-II blades were moved in one by one is shown in Fig. 19. The ratio of the voltage output from the blade monitor to that from the wall/liner monitor for this set of experiments is almost constant, as shown in Fig. 20, and we find $R_{Lw} = \Gamma_o(L)/\Gamma_o(w) \approx 20$.

The variations of $V_{out}(L)$ and $V_{out}(w)$ as a function of core plasma density when ALT-II was finally located at its nominal position of $a_\ell = 46$ cm are shown in Fig. 21. Let us estimate the particle fluxes during the stationary phase of the discharge. In this case the particle recycling coefficient $R = 1$, since there is no external source and no rate of change in plasma density. From the figures, we have $V_{out}(w) = 0.85$ V from the wall/liner monitor, which has an aperture of $D_w = 19$ mm, and from the blade/limiter monitor, with an aperture of $D_L = 10$ mm, we get $V_{out}(L) = 2.5$ V. From Eqs. (36) and (37) we then find

$$\Gamma_o(w) = 5 \times 10^{15}\ \mathrm{cm}^{-2} \cdot \mathrm{s}^{-1}\ , \tag{38}$$

$$\Gamma_o(L) = 1 \times 10^{17}\ \mathrm{cm}^{-2} \cdot \mathrm{s}^{-1}\ , \tag{39}$$

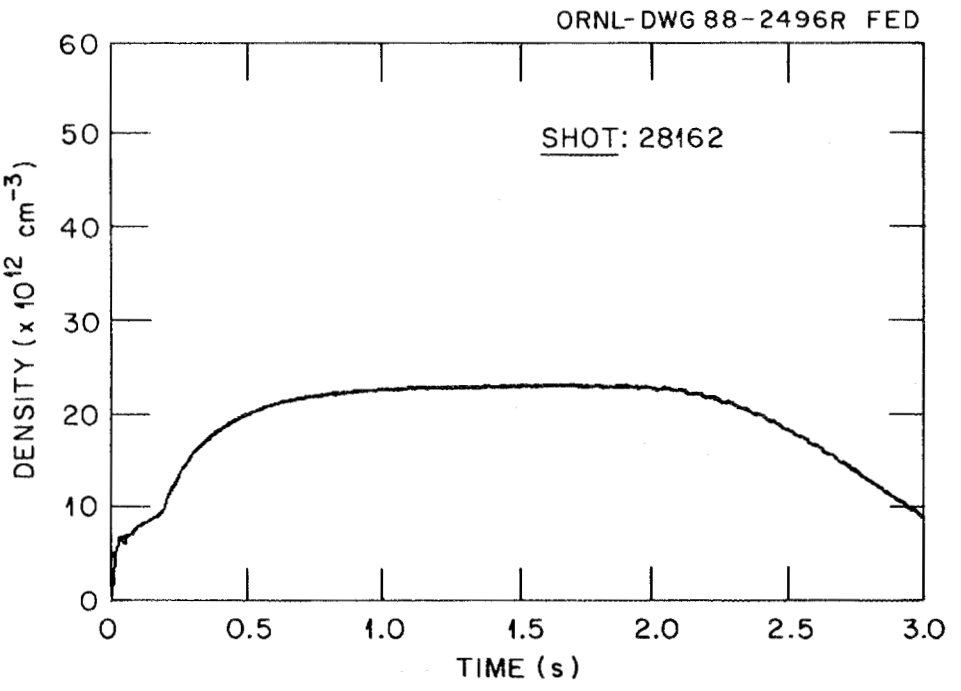

Fig. 18. Typical plasma density during the TEXTOR discharge.

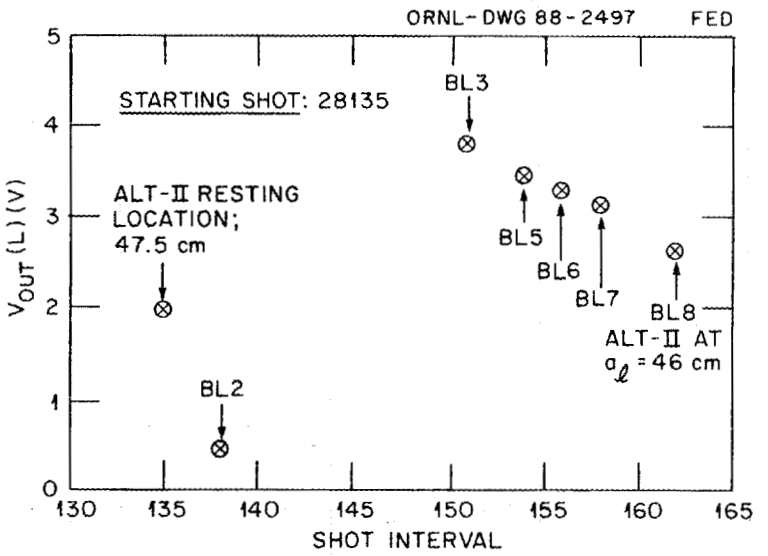

Fig. 19. Measured output voltage, $V_{\mathrm{out}}(\mathrm{L})$, of the limiter monitor as the ALT-II blades are moved in one by one.

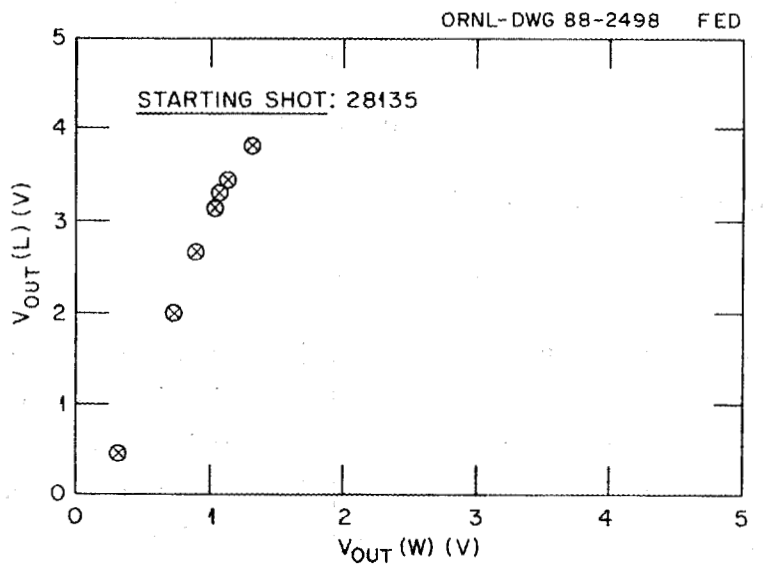

Fig. 20. Measured output voltage, $V_{\mathrm{out}}(\mathrm{L})$, of blade/limiter monitor as a function of output voltage, $V_{\mathrm{out}}(\mathrm{w})$, of the wall/liner monitor.

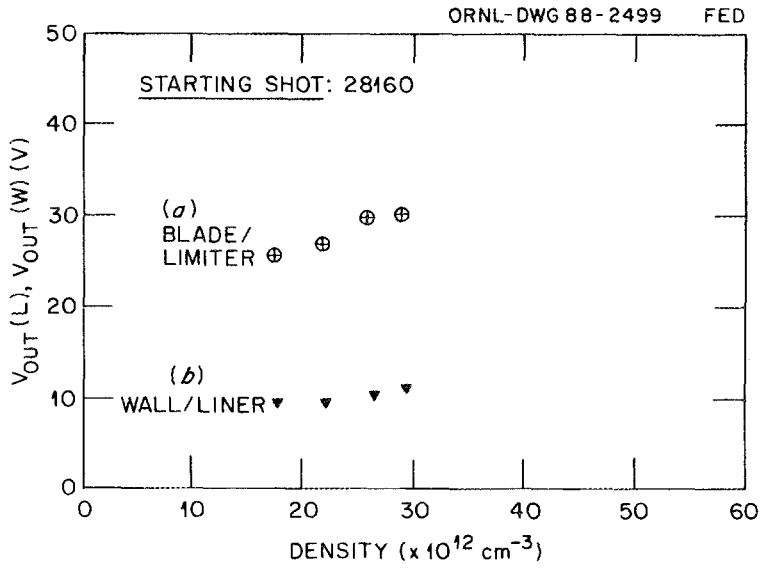

Fig. 21. (a) Measured output voltage, $V_{\rm out}$(L), of the blade/limiter monitor, and (b) output voltage, $V_{\rm out}$(w), of the wall/liner monitor, as a function of plasma density.

and from Eq. (20) we get the poloidal edge flux,

$$\Gamma_\theta = 2.45 \times 10^{17}\ \mathrm{cm}^{-2} \cdot \mathrm{s}^{-1}\ . \tag{40}$$

Using this value in Eq. (32) for a safety factor $q = 3.5$ gives

$$\Gamma_\parallel = 3.27 \times 10^{18}\ \mathrm{cm}^{-2} \cdot \mathrm{s}^{-1}\ . \tag{41}$$

We can also estimate this quantity from Eq. (33) by using the measured edge plasma parameters, $n_e = 1.7 \times 10^{12}$ cm^{-3} and $T_e = 25$–30 eV; for this case $\Gamma_\parallel$(calculation) = 3.4×10^{18} cm^{-2}·s^{-1}. Finally, for $\lambda_\Gamma = 1$ cm and a limiter connection length $L_c = 1925$ cm, and using the flux values given by Eqs. (38) and (41) in Eq. (30), we obtain the radial particle flux that is leaving the core plasma to the edge,

$$\Gamma_\perp(x = 0) = 6.7 \times 10^{15}\ \mathrm{cm}^{-2} \cdot \mathrm{s}^{-1}\ ; \tag{42}$$

using this value in Eq. (34) with $\lambda_n = \lambda_\Gamma$, we find $D_\perp = 4000$ cm·s^{-1}, which is the value estimated for the TEXTOR boundary plasma.[13]

The global particle confinement time, which is given by Eq. (27), can now be readily estimated. We assume a parabolic density profile, which gives $N_e = 1.37 \times 10^{20}$ particles for the core plasma volume of $V_p = 7.3 \times 10^6$ cm^3, and take the core plasma area to be $A_\perp(x = 0) = 3.178 \times 10^5$ cm^2. With these values and Eq. (42), we find the plasma efflux $\phi_\perp = 2.1 \times 10^{21}$ s^{-1}. Thus, the global particle confinement time is about $\tau_p = 65$ ms, which is consistent with earlier results obtained from the edge Langmuir probe measurements.[14]

IX. DISCUSSIONS

The H_α monitor system installed on TEXTOR is now ready for the next phase of ALT-II experiments with high auxiliary heating power. During these experiments the ALT-II pumping system will also be activated. The results from the H_α monitor system will contribute to the understanding of the toroidal belt pump limiter and its effects on the confinement characteristics of the TEXTOR core and edge plasmas. To carry out this task effectively, results from the other core and edge diagnostics in TEXTOR need to be correlated with the H_α measurements. Examples are the measurements of the edge plasma properties with the lithium beam, the ALT-II Langmuir probe, and the other optical edge diagnostics. We also hope to see the H_α monitor system used not only in the ALT-II experiments but also in the other experimental programs on TEXTOR, such as core plasma confinement studies. Specific areas include measurements of H-mode/L-mode confinement properties, characterization of attached/deattached plasmas, and ICH/NBI heating experiments.

Similar H_α monitors are being used on the Advanced Toroidal Facility[15] at ORNL.

REFERENCES

1. P. K. Mioduszewski et al., "Particle Removal with Pump Limiters in ISX-B," *J. Nucl. Mater.* **121**, 285 (1984).

2. K. H. Dippel et al., "ALT-I Pump Limiter Results on TEXTOR," in *Proc. 10th Int. Conf. Plasma Physics and Controlled Fusion Reasarch, London, 1984,* vol. 1, p. 249, International Atomic Energy Agency, Vienna, 1985.

3. R. W. Conn et al., "An Advanced Pump Limiter Experiment of Large Toroidal Extent–ALT-II," *J. Nucl. Mater.* **121**, 350 (1984).

4. K. H. Dippel et al., "Plasma-Wall Interactions and Plasma Performance in TEXTOR—A Review," *J. Nucl. Mater.* **145–147**, 3 (1987).

5. D. M. Goebel, private communication, 1987.

6. Oriel Corporation, Stamford, Conn.

7. L. Owen, T. Uckan, et al., "Experiments and Modelling of H_α Emission in TEXTOR with ALT-II Pump Limiter," in preparation.

8. D. Heifetz et al., "A Monte-Carlo Model of Neutral-Particle Transport in Diverted Plasmas," *J. Comput. Phys.* **46**, 309 (1982).

9. H. W. Darwin, "Spectroscopic Plasma Diagnostics," p. 519 in *Atomic and Molecular Physics of Controlled Thermonuclear Fusion,* C. J. Joachain and D. Post, eds., Plenum Press, New York, 1983.

10. W. E. Wiese, M. W. Smith, and B. M. Glennon, *Atomic Transition Probabilities: A Critical Data Compilation,* National Bureau of Standards Spec. Publ. 4, U.S. Government Printing Office, Washington, D.C., 1966.

11. EG&G, Inc., Electronic Products Division, Boston, Mass.

12. R. W. Conn et al., "Tokamak Pump Limiters," *J. Nucl. Mater.* **128 & 129**, 407 (1984).

13. U. Samm et al., "Structure of the Scrape-Off Layer and Particle Fluxes in a Limiter Tokamak," *J. Nucl. Mater.* **145–147**, 206 (1987).

14. D. M. Goebel et al., "Langmuir Probe Measurements in the TEXTOR Tokamak During ALT-I Pump Limiter Experiments," *Plasma Phys. Controlled Fusion* **29**, 473 (1987).

15. J. F. Lyon et al., "The Advanced Toroidal Facility," *Fusion Technol.* **10**, 179 (1986).

ORNL/TM-10698
Dist. Category UC-421, 424, 426

INTERNAL DISTRIBUTION

1. L. A. Berry
2. R. A. Dory
3. G. R. Dyer
4. J. L. Dunlap
5. J. H. Harris
6. D. L. Hillis
7. J. T. Hogan
8. R. C. Isler
9. C. C. Klepper
10. J. F. Lyon
11. P. K. Mioduszewski
12. O. B. Morgan
13. M. Murakami
14. G. H. Neilson
15. L. W. Owen
16. M. J. Saltmarsh
17. J. Sheffield
18. N. A. Uckan

19–31. T. Uckan

32–33. Laboratory Records Department

34. Laboratory Records, ORNL-RC
35. Document Reference Section
36. Central Research Library
37. Fusion Energy Division Library

38–39. Fusion Energy Division Publications Office

40. ORNL Patent Office

EXTERNAL DISTRIBUTION

41. Office of the Assistant Manager for Energy Research and Development, U.S. Department of Energy, Oak Ridge Operations Office, P. O. Box E, Oak Ridge, TN 37831
42. J. D. Callen, Department of Nuclear Engineering, University of Wisconsin, Madison, WI 53706-1687
43. J. F. Clarke, Director, Office of Fusion Energy, Office of Energy Research, ER-50 Germantown, U.S. Department of Energy, Washington, DC 20545
44. R. W. Conn, Department of Chemical, Nuclear, and Thermal Engineering, University of California, Los Angeles, CA 90024
45. S. O. Dean, Fusion Power Associates, Inc., 2 Professional Drive, Suite 249, Gaithersburg, MD 20760
46. H. K. Forsen, Bechtel Group, Inc., Research Engineering, P. O. Box 3965, San Francisco, CA 94105
47. J. R. Gilleland, Lawrence Livermore National Laboratory, P.O. Box 5511, Livermore, CA 94550
48. R. W. Gould, Department of Applied Physics, California Institute of Technology, Pasadena, CA 91125
49. R. A. Gross, Plasma Research Laboratory, Columbia University, New York, NY 10027

50. D. M. Meade, Princeton Plasma Physics Laboratory, P.O. Box 451, Princeton, NJ 08544
51. M. Roberts, International Programs, Office of Fusion Energy, Office of Energy Research, ER-52 Germantown, U.S. Department of Energy, Washington, DC 20545
52. W. M. Stacey, School of Nuclear Engineering and Health Physics, Georgia Institute of Technology, Atlanta, GA 30332
53. D. Steiner, Nuclear Engineering Department, NES Building, Tibbetts Avenue, Rensselaer Polytechnic Institute, Troy, NY 12181
54. R. Varma, Physical Research Laboratory, Navrangpura, Ahmedabad 380009, India
55. Bibliothek, Max-Planck Institut für Plasmaphysik, Boltzmannstrasse 2, D-8046 Garching, Federal Republic of Germany
56. Bibliothek, Institut für Plasmaphysik, KFA Jülich GmbH, Postfach 1913, D-5170 Jülich, Federal Republic of Germany
57. Bibliothek, KfK Karlsruhe GmbH, Postfach 3640, D-7500 Karlsruhe 1, Federal Republic of Germany
58. Bibliothèque, Centre de Récherches en Physique des Plasmas, Ecole Polytechnique Federale de Lausanne, 21 Avenue des Bains, CH-1007 Lausanne, Switzerland
59. F. Prévot, CEN/Cadarache, Departement de Récherches sur la Fusion Contrôlée, F-13108 Saint-Paul-lez-Durance Cedex, France
60. Bibliothèque, CEN/Cadarache, F-13108 Saint-Paul-lez-Durance Cedex, France
61. Library, Culham Laboratory, UKAEA, Abingdon, Oxfordshire, OX14 3DB, England
62. Library, JET Joint Undertaking, Abingdon, Oxfordshire, OX14 3EA, England
63. Library, FOM-Instituut voor Plasmafysica, Rijnhuizen, P.O. Box 1207, NL-3430 BE Nieuwegein, The Netherlands
64. Library, Institute of Plasma Physics, Nagoya University, Chikusa-ku, Nagoya 464, Japan
65. Library, International Centre for Theoretical Physics, P.O. Box 586, I-34100 Trieste, Italy
66. Library, Centro Richerche Energia Frascati, C.P. 65, I-00044 Frascati (Roma), Italy
67. Library, Plasma Physics Laboratory, Kyoto University, Gokasho, Uji, Kyoto, Japan
68. Plasma Research Laboratory, Australian National University, P.O. Box 4, Canberra, A.C.T. 2601, Australia
69. Thermonuclear Library, Japan Atomic Energy Research Institute, Tokai Establishment, Tokai-mura, Naka-gun, Ibaraki-ken, Japan
70. Library, Japan Atomic Energy Research Institute, Naka Fusion Research Establishment, Naka-machi, Naka-gun, Ibaraki-ken 311-02, Japan

71. G. A. Eliseev, I. V. Kurchatov Institute of Atomic Energy, P. O. Box 3402, 123182 Moscow, U.S.S.R.
72. V. A. Glukhikh, Scientific-Research Institute of Electro-Physical Apparatus, 188631 Leningrad, U.S.S.R.
73. I. Shpigel, Institute of General Physics, U.S.S.R. Academy of Sciences, Ulitsa Vavilova 38, Moscow, U.S.S.R.
74. D. D. Ryutov, Institute of Nuclear Physics, Siberian Branch of the Academy of Sciences of the U.S.S.R., Sovetskaya St. 5, 630090 Novosibirsk, U.S.S.R.
75. V. T. Tolok, Kharkov Physical-Technical Institute, Academical St. 1, 310108 Kharkov, U.S.S.R.
76. Library, Academia Sinica, P.O. Box 3908, Beijing, China (PRC)
77. R. A. Blanken, Experimental Plasma Research Branch, Division of Applied Plasma Physics, Office of Fusion Energy, Office of Energy Research, ER-542, Germantown, U.S. Department of Energy, Washington, DC 20545
78. K. Bol, Princeton Plasma Physics Laboratory, P.O. Box 451, Princeton, NJ 08544
79. R. A. E. Bolton, IREQ Hydro-Quebec Research Institute, 1800 Montee Ste.-Julie, Varennes, P.Q. JOL 2P0, Canada
80. D. H. Crandall, Experimental Plasma Research Branch, Division of Applied Plasma Physics, Office of Fusion Energy, Office of Energy Research, ER-542, Germantown, U.S. Department of Energy, Washington, DC 20545
81. R. L. Freeman, GA Technologies, Inc., P.O. Box 85608, San Diego, CA 92138
82. K. W. Gentle, RLM 11.222, Institute for Fusion Studies, University of Texas, Austin, TX 78712
83. R. J. Goldston, Princeton Plasma Physics Laboratory, P.O. Box 451, Princeton, NJ 08544
84. J. C. Hosea, Princeton Plasma Physics Laboratory, P.O. Box 451, Princeton, NJ 08544
85. S. W. Luke, Division of Confinement Systems, Office of Fusion Energy, Office of Energy Research, ER-55, Germantown, U.S. Department of Energy, Washington, DC 20545
86. E. Oktay, Division of Confinement Systems, Office of Fusion Energy, Office of Energy Research, ER-55, Germantown, U.S. Department of Energy, Washington, DC 20545
87. D. Overskei, GA Technologies, Inc., P.O. Box 85608, San Diego, CA 92138
88. R. R. Parker, Plasma Fusion Center, NW 16-288, Massachusetts Institute of Technology, Cambridge, MA 02139
89. W. L. Sadowski, Fusion Theory and Computer Services Branch, Division of Applied Plasma Physics, Office of Fusion Energy, Office of Energy Research, ER-541, Germantown, U.S. Department of Energy, Washington, DC 20545
90. J. W. Willis, Division of Confinement Systems, Office of Fusion Energy, Office of Energy Research, ER-55, Germantown, U.S. Department of Energy, Washington, DC 20545

91. A. P. Navarro, Division de Fusion Termonuclear, EURATOM/CIEMAT, Avenida Complutense 22, E-28040 Madrid, Spain
92. Laboratory for Plasma and Fusion Studies, Department of Nuclear Engineering, Seoul National University, Shinrim-dong, Gwanak-ku, Seoul 151, Korea
93. R. T. McGrath, Sandia National Laboratories, Albuquerque, NM 87175
94. J. B. Whitley, Sandia National Laboratories, Albuquerque, NM 87175
95. R. Aymar, Centre D'Etudes Nucléaires de Cadarache, B.P. No. A1, 13108 Saint Paul-lez-Durance Cedex, France
96. R. Deschamps, Centre d'Etudes Nucléaires de Cadarache, B.P. No. A1, 13108 Saint Paul-lez-Durance Cedex, France
97. R. Gravier, Centre d'Etudes Nucléaires de Cadarache, B.P. No. A1, 13108 Saint Paul-lez-Durance Cedex, France
98. D. Grossman, Centre d'Etudes Nucléaires de Cadarache, B.P. No. A1, 13108 Saint Paul-lez-Durance Cedex, France
99. D. Markevich, Advanced Fusion Concepts Branch, Division of Applied Plasma Physics, Office of Fusion Energy, Office of Energy Research, ER-543 Germantown, U.S. Department of Energy, Washington, DC 20545
100. K. H. Dippel, KFA Jülich, Postfach 1913, D-5170 Jülich 1, Federal Republic of Germany

101–156. Given distribution according to TIC-4500, Magnetic Fusion Energy (Category UC-421, 424, 426: Plasma Fusion Systems, Magnetic Fusion Energy Systems, Experimental Plasma Physics)